

Fractional excitations in the square-lattice quantum antiferromagnet

B. Dalla Piazza^{1*}, M. Mourigal^{1,2,3*}, N. B. Christensen^{4,5}, G. J. Nilsen^{1,6}, P. Tregenna-Piggott⁵, T. G. Perring⁷, M. Enderle², D. F. McMorrow⁸, D. A. Ivanov^{9,10} and H. M. Rønnow^{1,11}

Quantum magnets have occupied the fertile ground between many-body theory and low-temperature experiments on real materials since the early days of quantum mechanics. However, our understanding of even deceptively simple systems of interacting spin-1/2 particles is far from complete. The quantum square-lattice Heisenberg antiferromagnet, for example, exhibits a striking anomaly of hitherto unknown origin in its magnetic excitation spectrum. This quantum effect manifests itself for excitations propagating with the specific wavevector $(\pi, 0)$. We use polarized neutron spectroscopy to fully characterize the magnetic fluctuations in the metal-organic compound $\text{Cu}(\text{DCOO})_2 \cdot 4\text{D}_2\text{O}$, a known realization of the quantum square-lattice Heisenberg antiferromagnet model. Our experiments reveal an isotropic excitation continuum at the anomaly, which we analyse theoretically using Gutzwiller-projected trial wavefunctions. The excitation continuum is accounted for by the existence of spatially extended pairs of fractional $S=1/2$ quasiparticles, 2D analogues of 1D spinons. Away from the anomalous wavevector, these fractional excitations are bound and form conventional magnons. Our results establish the existence of fractional quasiparticles in the high-energy spectrum of a quasi-two-dimensional antiferromagnet, even in the absence of frustration.

A fascinating manifestation of quantum mechanics is the emergence of elementary excitations carrying fractional quantum numbers. Fractional excitations were a central ingredient to understand the fractional quantum Hall effect¹, and have been investigated in a range of systems, including conducting polymers², bilayer graphene³, cold atomic gases⁴ and low-dimensional quantum magnets^{5,6}. Among the latter class of systems, the spin-1/2 Heisenberg antiferromagnet chain (HAFc) is perhaps the simplest model for which the ground state and the excitations are known exactly^{7–9}. Excitations of the spin-1/2 HAFc created by an elementary $\Delta S=1$ process are radically different from spin waves, the coherent propagation of a flipped spin, and are pairs of unbound fractional quasiparticles known as spinons, each carrying a $S=1/2$ quantum number. The existence of spinons in the spin-1/2 HAFc has been confirmed experimentally in a number of quasi-1D materials^{10,11}, but observing their 2D and 3D analogues is an ongoing challenge⁶. So far, the main candidate systems comprise geometrically frustrated magnets on the triangular¹² or kagome^{13–15} lattices. In this work, we take a frustration-free route and focus on the quantum (spin-1/2) square-lattice Heisenberg antiferromagnet (QSLHAF), one of the most fundamental models in magnetism. It is defined by the Hamiltonian

$$\mathcal{H} = J \sum_{\langle i,j \rangle} \mathbf{S}_i \cdot \mathbf{S}_j \quad (1)$$

where J is the antiferromagnetic exchange interaction between nearest-neighbour spins described by spin $S=1/2$ operators \mathbf{S}_i and \mathbf{S}_j . We provide experimental and theoretical evidence that

even in this simplest of 2D models deconfined fractional $S=1/2$ quasiparticles can be identified at high energies, where they modify the short-wavelength spin dynamics and are responsible for a significant quantum anomaly that cannot be captured by conventional spin-wave theory.

It may seem surprising that the QSLHAF is a candidate for hosting fractional excitations, as at a superficial level its long-range magnetic order resembles that of a classical system. The elementary excitations of this ‘Néel state’, when calculated using semi-classical spin-wave theory (SWT), are bosonic quasiparticles, known as magnons: the one-magnon spectrum is gapless, with two-magnon excitations occupying a continuum at higher energy. The interaction between magnons is relatively weak and leads to an upward renormalization of the magnon energy and to scattering between two-magnon states^{16,17}. One- and two-magnon excitations, respectively, correspond to fluctuations perpendicular (transverse) and parallel (longitudinal) to the direction of the ordered moments.

Although none of the above properties suggest the existence of quasiparticle fractionalization, quantum effects are nevertheless far from negligible in the QSLHAF. This is evidenced by the observation that quantum zero-point fluctuations reduce the staggered moment to only 62% of its fully ordered value $S=1/2$ (refs 18,19). This suggests that the QSLHAF may in fact be close to a state preserving spin-rotation symmetry, such as the resonating-valence-bond (RVB) state proposed by Anderson²⁰ for the cuprate realization of this model. In particular, fractional spin excitations present in the RVB state may be relevant for the spin dynamics in the Néel state, especially at high energies. Indeed, analytical theories

¹Laboratory for Quantum Magnetism, École Polytechnique Fédérale de Lausanne (EPFL), CH-1015, Switzerland. ²Institut Laue-Langevin, BP 156, F-38042 Grenoble Cedex 9, France. ³Institute for Quantum Matter and Department of Physics and Astronomy, Johns Hopkins University, Baltimore, Maryland 21218, USA. ⁴Department of Physics, Technical University of Denmark (DTU), DK-2800 Kgs. Lyngby, Denmark. ⁵Laboratory for Neutron Scattering, Paul Scherrer Institute, CH-5232 Villigen PSI, Switzerland. ⁶Department of Chemistry, University of Edinburgh, Edinburgh EH9 3JJ, UK. ⁷ISIS Facility, Rutherford Appleton Laboratory, Chilton, Didcot, Oxon OX11 0QX, UK. ⁸London Centre for Nanotechnology and Department of Physics and Astronomy, University College London, London WC1H 0AH, UK. ⁹Institute for Theoretical Physics, ETH Zürich, CH-8093 Zürich, Switzerland. ¹⁰Institute for Theoretical Physics, University of Zürich, CH-8057 Zürich, Switzerland. ¹¹RIKEN Centre for Emergent Matter Science (CEMS), Wako 351-0198, Japan.

*e-mail: bastien.dallapiazza@epfl.ch; mourigal@gatech.edu

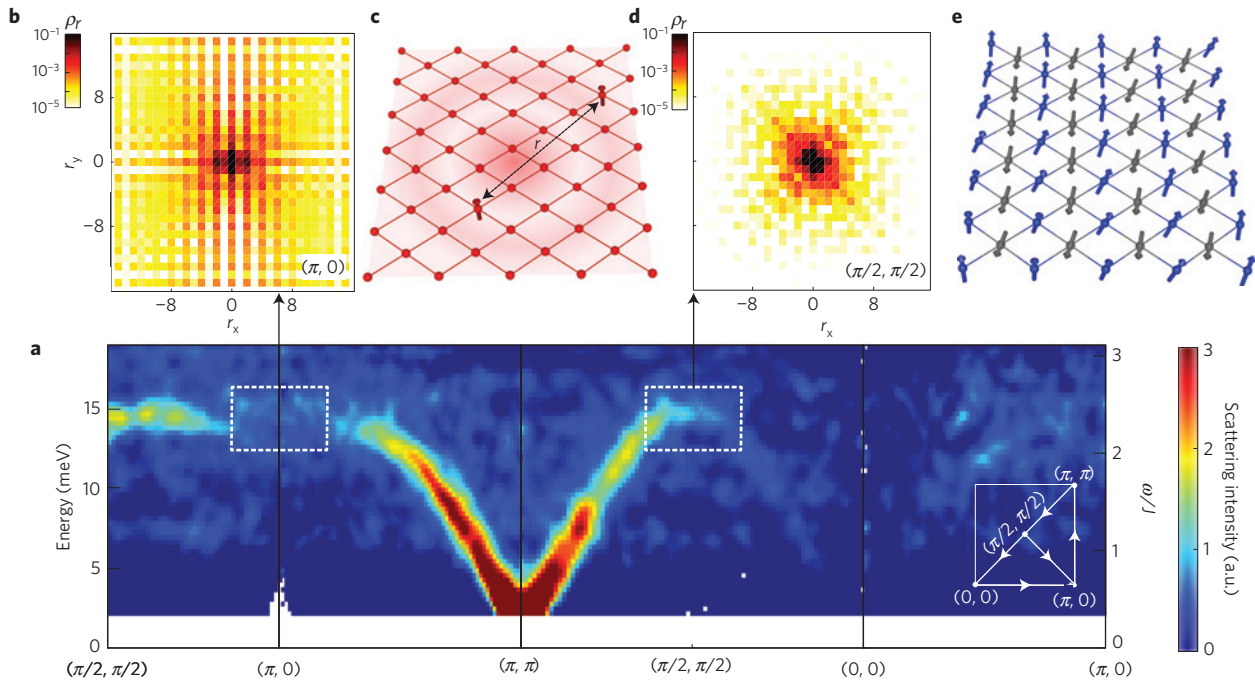


Figure 1 | Overview of the magnetic excitation spectrum of CFTD and its interpretation in terms of spin waves or spatially extended fractional excitations. a, Momentum and energy dependence of the (total) dynamic structure factor $\mathcal{S}(\mathbf{q}, \omega)$ measured by time-of-flight inelastic neutron scattering. Square boxes (black dashed) highlight the $(\pi, 0)$ and $(\pi/2, \pi/2)$ wavevectors. a.u., arbitrary units. **b,d**, Corresponding distributions of real-space fractional quasiparticle-pair separations, as calculated in the $|\text{SF}\rangle$ variational state (equation (3)), evidencing, respectively, the unbound and bound nature of the pair excitations. **c,e**, Pictorial representation of a quasiparticle-pair excitation and a spin-wave excitation (magnon), respectively.

using bosonic²¹ or fermionic^{22,23} fractional quasiparticles have long been proposed, and it has been shown that the presence of conventional classical long-range order does not hinder the possibility of fractional excitations^{24,25}. By analogy with the 1D case, these are referred to as spinons.

The magnetic excitation spectrum of various realizations of the QSLHAF have been investigated using neutron spectroscopy, including the parent compounds of the high- T_c cuprate superconductors $\text{Sr}_2\text{CuO}_2\text{Cl}_2$ (refs 26,27) and La_2CuO_4 (refs 28,29), $\text{Sr}_2\text{Cu}_3\text{O}_4\text{Cl}_2$ (ref. 30) and the metal-organic compounds $\text{Cu}(\text{pz})_2(\text{ClO}_4)_2$ (refs 31,32) and $\text{Cu}(\text{DCCO})_2 \cdot 4\text{D}_2\text{O}$ (CFTD; refs 33,34) considered here. These experiments have established that, although SWT gives an excellent account of the low-energy spectrum, a glaring anomaly is present at high energy for wavevectors \mathbf{q} in the vicinity of $(\pi, 0)$, where $\mathbf{q} = (q_x, q_y)$ is expressed in the square-lattice Brillouin zone of unit length 2π . The anomaly is evident as a complete wipe out of intensity (Fig. 1a) of the otherwise sharp excitations^{27,29,32,34} and as a 7% downward dispersion along the magnetic zone boundary connecting the $(\pi/2, \pi/2)$ and $(\pi, 0)$ wavevectors for $\text{Sr}_2\text{Cu}_3\text{O}_4\text{Cl}_2$ (refs 30,33) and CFTD. Unambiguously identifying the origin of this effect is complicated by the presence, in some of these materials, of further small exchange terms such as electronic ring-exchange^{27,29}, further neighbour exchange^{31,32} or interpenetrating sublattices³⁰. In contrast, the deviations observed in CFTD agree with numerical results obtained by series expansion^{35,36}, quantum Monte Carlo^{37,38} and exact diagonalization³⁹ methods for the model of equation (1), proving that the anomaly is in this case intrinsic³⁴. Owing to the similarities of the measured anomaly to some aspects of the predicted fermionic RVB excitations treated in the random phase approximation²³, it has been speculated that the anomaly might be related to fractionalized spin excitations^{29,34}. Given the greatly enlarged family of experimentally accessible physical realizations of QSLHAF owing to the advent of high-resolution resonant inelastic

X-ray scattering^{40–43} and the fundamental nature of the QSLHAF, it is clearly desirable to develop a microscopic understanding of the origin of the anomaly.

Here we present polarized neutron scattering results on CFTD which establish the existence of a spin-isotropic continuum at $(\pi, 0)$, which contrasts sharply with the dominantly longitudinal continuum at $(\pi/2, \pi/2)$ and with the broken spin symmetry of the ground state. Using a fermionic description of the spin dynamics based on a Gutzwiller-projected variational approach, we argue that the continuum at $(\pi, 0)$ is a signature of spatially extended pairs of fractional $S = 1/2$ quasiparticles (Fig. 1b,c). At other wavevectors, including $(\pi/2, \pi/2)$ (Fig. 1d), our approach yields bound pairs of these fractional quasiparticles and so recovers a conventional magnon spectrum, in agreement with SWT (Fig. 1e).

Neutron scattering experiments were performed on single crystals of CFTD using unpolarized time-of-flight spectroscopy (Fig. 1) and triple-axis spectroscopy with longitudinal polarization analysis (see Supplementary Methods). The results of our polarized experiment are presented in Fig. 2 through the energy dependence ω of the diagonal components of the dynamic structure factor $\mathcal{S}(\mathbf{q}, \omega)$. By combining wavevectors from different equivalent Brillouin zones (see Supplementary Methods), we can reconstruct the total dynamic structure factor (Fig. 2a,e), and separate contributions from spin fluctuations that are transverse to and along (Fig. 2b,c,f,g) the ordered moment. Within SWT, the resulting transverse and longitudinal spectra are dominated by one-magnon and two-magnon excitations, respectively. At $(\pi/2, \pi/2)$, and at an excitation energy of $\omega = 2.38(2) J$, we observe a sharp, energy resolution-limited peak ($\Delta\omega = 1.47(5) \text{ meV} = 0.24(1) J$, FWHM) which is the signature of a long-lived, single-particle excitation (Fig. 2e). Most of the observed spectral weight is in the resolution-limited peak of the transverse channel $\mathcal{S}^\perp(\mathbf{q}, \omega) \equiv \mathcal{S}^{xx}(\mathbf{q}, \omega) + \mathcal{S}^{yy}(\mathbf{q}, \omega)$ (Fig. 2f), while a weak continuum extends from $\omega/J \approx 2.3$ to 3.4, with a maximum around $\omega/J \approx 2.6$ in the longitudinal channel, $\mathcal{S}^{zz}(\mathbf{q}, \omega)$

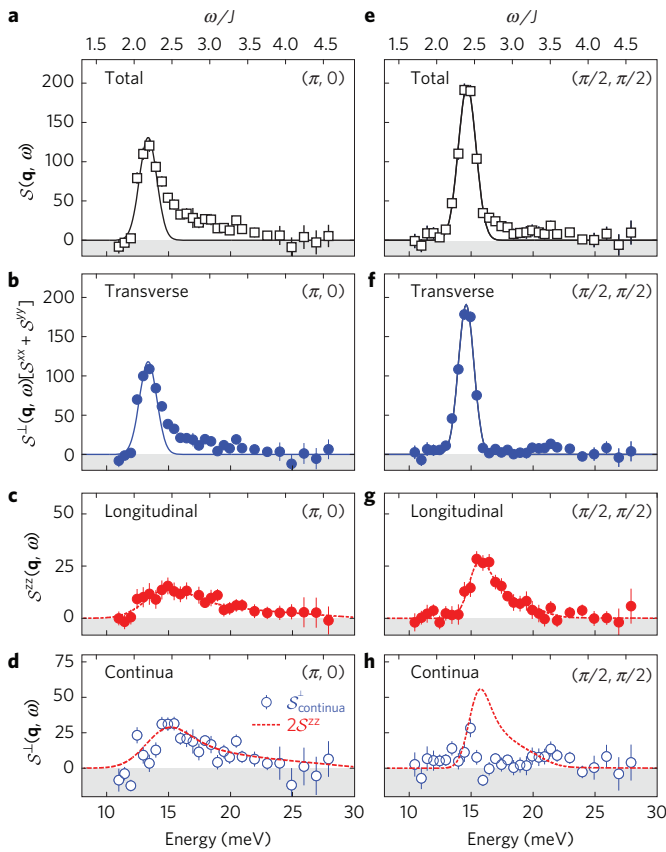


Figure 2 | Summary of the polarized neutron scattering data.

a-c, e-g. Energy dependence of the total, transverse and longitudinal contributions to the dynamic structure factor, respectively, at constant wavevectors $\mathbf{q} = (\pi, 0)$ (**a-c**) and $\mathbf{q} = (\pi/2, \pi/2)$ (**e-g**) measured by polarized neutron scattering on CFTD. The solid lines indicate resolution-limited Gaussian fits, while the dashed lines are empirical lineshapes used as guides-to-the-eye. **d, h.** Transverse dynamic structure factor with subtracted resolution-limited Gaussian fits at $(\pi, 0)$ and $(\pi/2, \pi/2)$, respectively. Error bars correspond to one standard deviation.

(Fig. 2g). In contrast, the response at $(\pi, 0)$ exhibits a pronounced high-energy tail, starting right above the peak maximum at $\omega/J = 2.19(2)$, and extending up to $\omega/J \approx 3.8$. This tail carries 40(12)% of the total spectral weight at $(\pi, 0)$ (Fig. 2a), and is evident in both the transverse (Fig. 2b) and longitudinal (Fig. 2c) channels. To isolate the continuous component in the transverse channel we subtract resolution-limited Gaussians corresponding to sharp, single-particle responses, with the results shown in Fig. 2d, h. This analysis reveals the important fact that the transverse continuum at $(\pi, 0)$ is within error twice the longitudinal contribution (Fig. 2d). Thus, we can conclude that the continuum at $(\pi, 0)$ arises from correlations which are isotropic in spin space, with $S^\perp(\mathbf{q}, \omega) = 2S^{zz}(\mathbf{q}, \omega)$, whereas by contrast the continuum contribution at $(\pi/2, \pi/2)$ is fully contained in the longitudinal channel (Fig. 2h).

The pronounced asymmetric and non-Lorentzian line shape of the continuum at $(\pi, 0)$ cannot be accounted for by conventional effects, even including instrumental resolution. SWT predicts that magnon interactions transfer up to 20% of the transverse spectral weight at the zone boundary from the sharp one-magnon peak to a higher energy continuum of three-magnon states¹⁷. However, the resulting line shape differs radically from our observations, does not coincide with the longitudinal response, and does not seem to depend significantly on the wavevector along the zone boundary. Spontaneous magnon decays can in principle produce

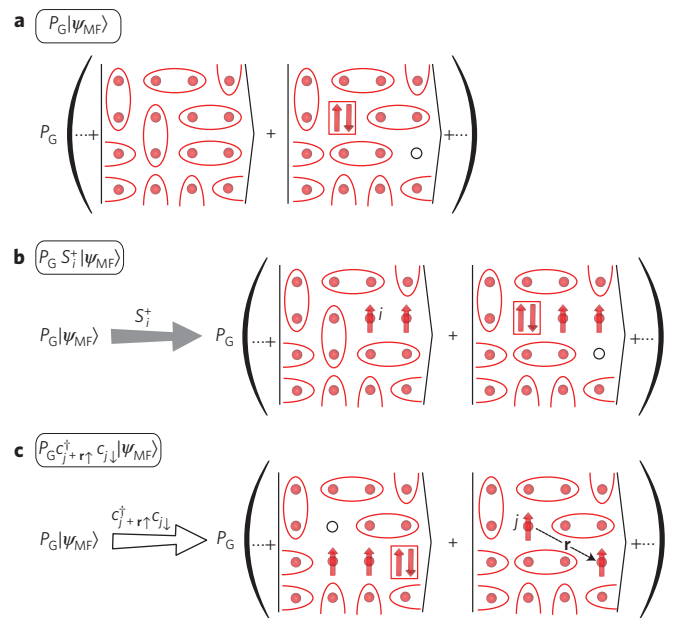


Figure 3 | Schematic representation of local spin flip and spatially separated quasiparticle-pair excitations in the Gutzwiller-projected approach.

a. The mean-field wavefunction $|\psi_{MF}\rangle$ is shown as a resonating-valence-bond liquid (for better visualization, all singlets are shown as nearest-neighbour and the Néel order is ignored). Configurations containing doubly occupied sites (right-hand side) are discarded by the Gutzwiller projection P_G . **b.** Local spin flips create triplets out of resonating singlets. Configurations from $|\psi_{MF}\rangle$ originally containing doubly occupied sites are still projected out (right-hand side). **c.** Non-local quasiparticle-pair excitations are constructed as projected particle-hole excitations. At a non-zero separation \mathbf{r} , they contribute by annihilating a doubly occupied site with a hole, leaving two separated spin ups. After projection, the only configurations left are the ones constructed from $|\psi_{MF}\rangle$ that contained one empty and one doubly occupied site (right-hand side).

an asymmetric line shape, but are prohibited in this case by the collinearity of the magnetic order^{16,44}. Instead, recent quantum Monte Carlo work⁴⁵ suggests looking for explanations of the continuum contribution to the dynamic structure factor at $(\pi, 0)$ involving the deconfinement of fractional excitations. This is further motivated by the observed coexistence of sharp two-spinon bound states with a broad multi-spinon continuum, at comparable energy ranges but different wavevectors, in the quasi-2D materials Cs_2CuCl_4 ^{12,46} and LiCuVO_4 ⁴⁷, made of strongly coupled Heisenberg chains.

To explore whether fractionalization of magnons can account for the $(\pi, 0)$ anomaly in the QSLHAF, we use a theoretical approach based on Gutzwiller-projected variational wavefunctions^{48,49}. In this approach, spin operators are transformed into pairs of $S = 1/2$ fermionic operators so that equation (1) becomes

$$\mathcal{H} = -\frac{J}{2} \sum_{(ij), \sigma, \sigma'} c_{i\sigma}^\dagger c_{j\sigma} c_{i\sigma'}^\dagger c_{j\sigma'} + \text{constant} \quad (2)$$

where $c_{i\sigma}^\dagger$ ($c_{i\sigma}$) creates (annihilates) an electron with spin σ at site i . This transformation embeds the original spin Hilbert space into an electronic Hilbert space which also contains non-magnetic sites occupied by zero or two electrons. As a result, equations (1) and (2) are only equivalent on the restricted electronic subspace with half electron filling and no empty sites or double occupancies. This constraint can be enforced exactly by the so-called Gutzwiller projector P_G . The advantage of this approach is that pairs of fractional $S = 1/2$ quasiparticles (for the original spin Hamiltonian) can be naturally constructed

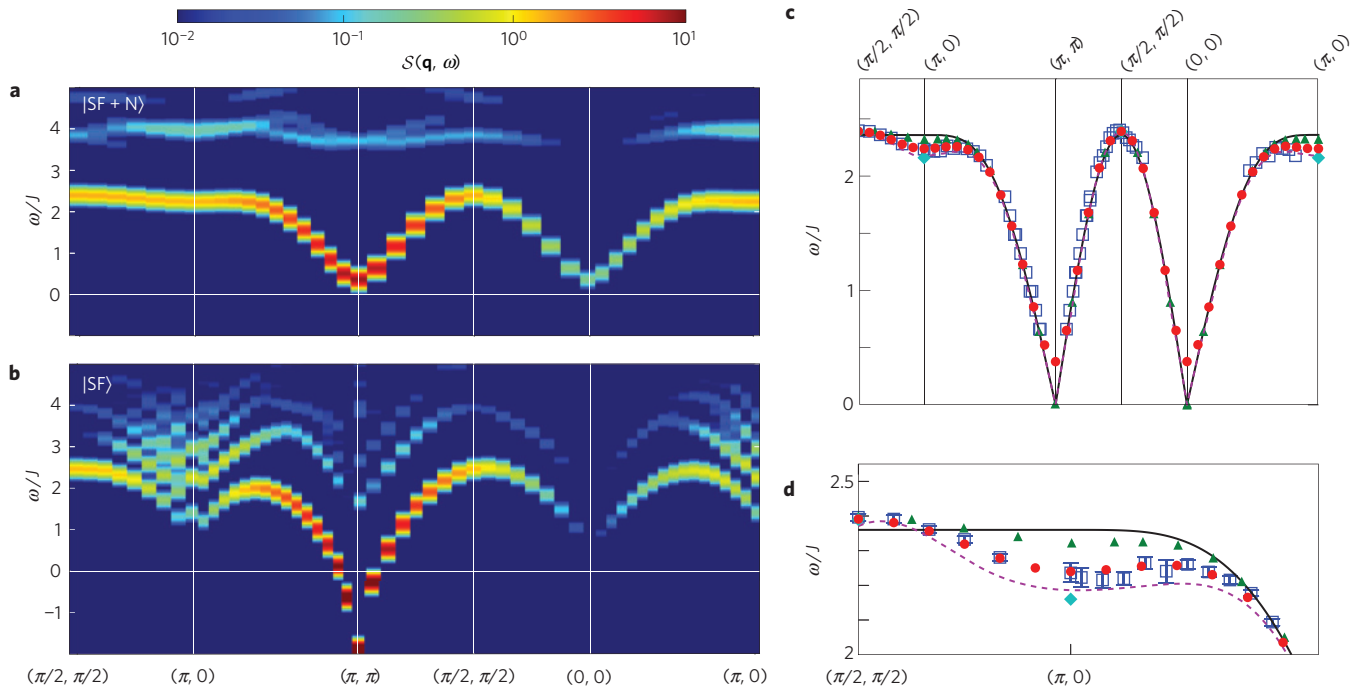


Figure 4 | Variational excitation spectra of the Gutzwiller-projected trial wavefunctions. **a, b**, Transverse dynamic structure factor for the $|\text{SF} + \text{N}\rangle$ (**a**) and $|\text{SF}\rangle$ (**b**) states with lattice sizes of 24×24 and 32×32 respectively. **c**, The magnon-like dispersion extracted from **a** (red points) compared to the experimental CFTD data³⁴ (blue squares, error bars correspond to one standard deviation), spin-wave theory with first-order (solid black line) and third-order⁶¹ (green triangles) $1/S$ corrections, series expansion³⁶ (dashed purple line) and quantum Monte Carlo³⁸ (cyan diamonds). The experimental data is scaled using $J = 6.11$ meV. **d**, Zoom-in on the magnon-like mode dispersion along the magnetic zone boundary.

as particle–hole excitations in the electronic space, projected a posteriori by P_G onto spin configurations with exactly one electron per site⁵⁰. The projection may be approximated using the Gutzwiller approximation²² or the random phase approximation²³. In this work we choose to implement the projection exactly using the numerical variational Monte Carlo technique⁴⁹. (The source code used to perform the variational Monte Carlo calculations is available at <https://github.com/epfl-lqm/gpvmc>.)

The quartic electronic operator in equation (2) is treated by a mean-field decoupling where the averages $\langle c_{i\sigma}^\dagger c_{i\sigma} \rangle$ and $\langle c_{i\sigma}^\dagger c_{j\sigma} \rangle$ are considered. We adopt the following Ansätze for their real-space dependencies: $\langle c_{i\sigma}^\dagger c_{i\sigma} \rangle$ corresponds to a staggered Néel order parameter (N) and $\langle c_{i\sigma}^\dagger c_{j\sigma} \rangle$ to a staggered flux (SF) threading square plaquettes of the lattice^{51–53} (see Supplementary Methods for exact definitions and more details). To each average corresponds a variational parameter whose value is optimized to minimize the energy (equation (1)) of the Gutzwiller-projected state, $|\text{SF} + \text{N}\rangle = P_G |\psi_{\text{MF}}\rangle$. The corresponding mean-field electronic ground-state $|\psi_{\text{MF}}\rangle$ contains empty and doubly occupied sites and reads

$$|\psi_{\text{MF}}\rangle = \prod_{\mathbf{k} \in \text{MBZ}} \gamma_{\mathbf{k}\uparrow}^\dagger \gamma_{\mathbf{k}\downarrow}^\dagger |0\rangle$$

where $|0\rangle$ is the electron vacuum and where the $\gamma_{\mathbf{k}\sigma\pm}^{(\dagger)}$ operators are linear combinations of $c_{\mathbf{k}\sigma}^{(\dagger)}$ operators that diagonalize the mean-field electronic Hamiltonian. The product over the wavevector \mathbf{k} is restricted to the magnetic Brillouin zone (MBZ), a result of the antiferromagnetic unit-cell-doubling. Consequently ‘ \pm ’ denotes the band index. In the present case of half electron filling, the ‘ $-$ ’ band is fully occupied, and there is a finite gap to the empty ‘ $+$ ’ band for non-zero Néel order parameter. The overall minimization procedure is carried out numerically using variational Monte Carlo and leads to a $|\text{SF} + \text{N}\rangle$ state with variational energy $E_{\text{SF}+\text{N}} = -0.664J$

and staggered moment $0.75S$ per site^{48,54}. This can be compared to more precise Green’s function Monte Carlo studies for equation (1) that obtained $-0.669J$ and $0.615S$ for the ground-state energy and the staggered moment, respectively^{55,56}.

The optimized $|\text{SF} + \text{N}\rangle$ state, although giving a good estimate for the ground-state energy, does not have the correct long-distance behaviour for the transverse equal-time correlator $\langle S^+(0)S^-(\mathbf{r}) \rangle$, predicted by SWT to decay as a power-law¹⁶. This algebraic decay is a robust long-wavelength prediction and has been implemented in variational magnetic trial wavefunctions in the past^{57,58}. Instead, as the excitation spectrum of the mean-field electronic ground state is gapped, $\langle S^+(0)S^-(\mathbf{r}) \rangle$ decays exponentially after projection. We conjecture that the asymptotic behaviour of the spin correlator is important for the deconfinement of fractional excitations. To obtain insight into the influence of long-distance spin fluctuations, we consider a distinct variational state, $|\text{SF}\rangle$, for which the finite staggered flux is retained but the Néel order is reduced to zero. $|\text{SF}\rangle$ is a quantum spin-liquid singlet of variational energy $E_{\text{SF}} = -0.638J$ that exhibits a power-law decay of its transverse spin correlations^{59,60}.

We now turn to the construction of transverse ($S = 1$) spin excitations for the above variational states, aiming at comparing their respective dynamic structure factor with the results of Fig. 2. The variational transverse spin excitations are obtained as superpositions of projected particle–hole excitations with momentum \mathbf{q} :

$$|\mathbf{q}, n, +\rangle = \sum_{\mathbf{k} \in \text{MBZ}} \phi_{\mathbf{k}\mathbf{q}}^n |\mathbf{k}, \mathbf{q}\rangle, \quad |\mathbf{k}, \mathbf{q}\rangle = P_G \gamma_{\mathbf{k}\uparrow}^\dagger \gamma_{\mathbf{k}-\mathbf{q}\downarrow} |\psi_{\text{MF}}\rangle$$

where the states $|\mathbf{k}, \mathbf{q}\rangle$ are generated by destroying a spin-down quasiparticle in the ‘ $-$ ’ band and creating a spin-up quasiparticle in the ‘ $+$ ’ band. The coefficients $\phi_{\mathbf{k}\mathbf{q}}^n$ are obtained by diagonalizing

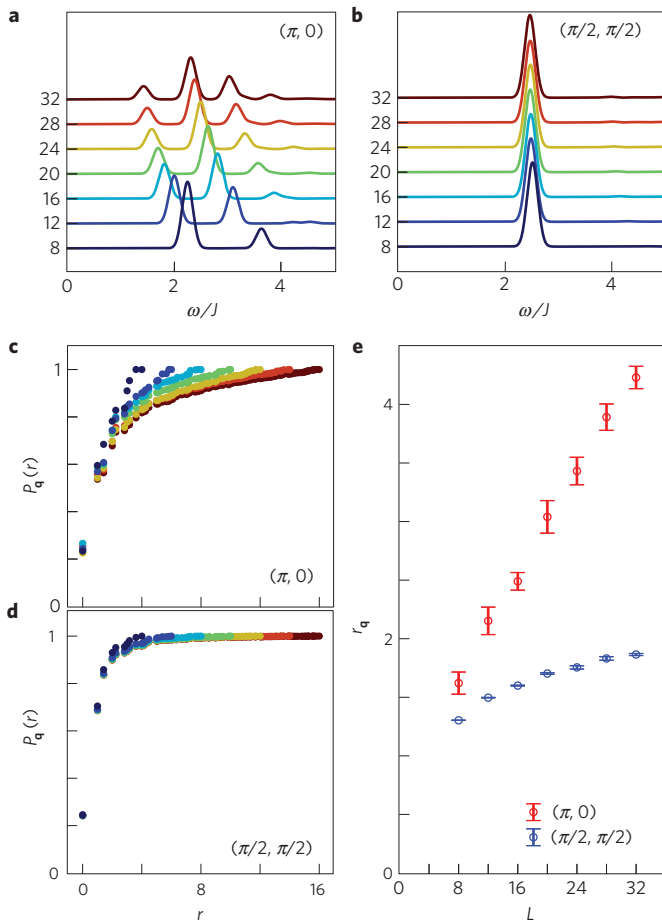


Figure 5 | Finite-size effects and real-space structure in the |SF> state.

a, b, Transverse dynamic spin structure factor at $(\pi, 0)$ (**a**) and $(\pi/2, \pi/2)$ (**b**) for different system sizes ranging from 8×8 (dark blue line) to 32×32 (dark red line). **c, d**, Disk-integrated fractional-quasiparticle-pair separation distribution $P_q(r)$ at $(\pi, 0)$ (**c**) and $(\pi/2, \pi/2)$ (**d**) for corresponding system sizes. **e**, Mean fractional-quasiparticle-pair separation r_q at $(\pi, 0)$ (red symbols) and $(\pi/2, \pi/2)$ (blue symbols). Error bars correspond to one standard deviation from the variational Monte Carlo sampling.

the original Hamiltonian (equation (1)) projected onto the non-orthonormal set of states $|\mathbf{k}, \mathbf{q}\rangle$ and correspond to the eigenenergies $E_{q_n}^+$. Expressing the Fourier-space quasiparticle operators $\gamma_{k\sigma\pm}$ using the real-space $c_{i\sigma}$ operators, we note that the variational spin excitations contain both local spin flips $S_i^+ P_G |\psi_{MF}\rangle = P_G c_{i\uparrow}^\dagger c_{i\downarrow} |\psi_{MF}\rangle$ (Fig. 3b) and spatially separated particle-hole excitations, $P_G c_{j+\mathbf{r}\uparrow}^\dagger c_{j\downarrow} |\psi_{MF}\rangle$ (Fig. 3c). The dynamic structure factor of the transverse spin excitations is calculated as

$$S^{+-}(\mathbf{q}, \omega) = \sum_n \left| \langle \mathbf{q}, n, + | S_q^+ | \text{GS} \rangle \right|^2 \delta(\omega - E_{q_n}^+ + E_{\text{GS}})$$

where |GS> stands either for |SF + N> or |SF>. We use the identity $S^\perp \equiv S^{+-} = S^{-+}$, valid for both variational ground states, to compare the transverse dynamic structure factor of the variational states |SF + N> and |SF> with the experimental results presented in Fig. 2. A similar approach also allows one to obtain the longitudinal ($S=0$) dynamic structure factor (see Supplementary Methods).

The transverse dynamic structure factor $S^\perp(\mathbf{q}, \omega)$ of the |SF + N> state is shown in Fig. 4a, as obtained by variational Monte Carlo on a finite lattice of 24×24 sites. The dominant feature of the spectrum is a low-energy magnon-like mode, which resembles

the experimental results of Fig. 1a. In particular, our calculation produces a dispersion along the magnetic zone boundary in better quantitative agreement with the 7% dispersion observed in ref. 34 than any other theoretical method (Fig. 4c,d). This confirms that magnons can be quantitatively interpreted as bound pairs of fractional $S=1/2$ quasiparticles.

However, the $|\text{SF} + \text{N}\rangle$ transverse dynamic structure factor exhibits a gap at (π, π) and no continuum above the magnon branch at $(\pi, 0)$. We believe that this is an artefact of replacing the spontaneous symmetry breaking by a Néel mean-field order parameter: this ansatz, as mentioned above, distorts the long-distance asymptotics of spin correlations. Indeed, if we reduce the Néel mean-field parameter of the $|\text{SF} + \text{N}\rangle$ state, then the high-energy excitations at $(\pi, 0)$ move down in energy (see Supplementary Methods). When the Néel field vanishes (that is, in the |SF> state), they evolve into a succession of modes distributed on an extended energy range above the spin-wave mode (shown in Fig. 4b for a 32×32 lattice). This behaviour contrasts the situation at $(\pi/2, \pi/2)$, where the high-energy transverse excitations completely lose their spectral weight on reducing the Néel field and only the spin-wave mode remains in the |SF> state. At (π, π) , the lowest mode moves down, reaching negative energy, which indicates an instability of the |SF> state towards Néel ordering. We therefore suggest that the continuum of excitations observed at $(\pi, 0)$ is conditionally dependent on power-law transverse spin correlations and that it corresponds to deconfined fractional spin-1/2 quasiparticles.

To support this interpretation, we consider in Fig. 5a,b the system-size dependence of $S^\perp(\mathbf{q}, \omega)$. Although the excitations at $(\pi/2, \pi/2)$ form a single sharp mode with energy and intensity nearly independent of the system size, the number of modes at $(\pi, 0)$ and their relative weights are strongly modified on increasing the number of sites. This behaviour is consistent with the development of a continuum of fractional quasiparticles at $(\pi, 0)$ in the thermodynamic limit.

Having established that our Gutzwiller approach depending on wavevector produces respectively sharp and continuum-like excitations from the |SF> state, we analyse their real-space structure to gain further insight into their nature. We consider their overlap with projected real-space particle-hole excitations $|\mathbf{q}, \mathbf{r}, +\rangle = P_G \sum_{\mathbf{R}} e^{i\mathbf{q}\cdot\mathbf{R}} c_{\mathbf{R}+\mathbf{r}\uparrow}^\dagger c_{\mathbf{R}\downarrow} |\psi_{MF}\rangle$, where a Fourier transformation was applied to reflect translation invariance. In this formalism, the most local projected particle-hole pair is the spin-flip state $S_q^+ |\text{SF}\rangle = |\mathbf{q}, 0, +\rangle$ corresponding to a magnon while non-local pairs are characterized by a finite separation \mathbf{r} . Therefore, the degree of deconfinement of a fractional $S=1/2$ quasiparticles pair can be characterized using the spatial extent of its overlap with projected real-space particle-hole excitations $\langle \mathbf{q}, \mathbf{r}, + | \mathbf{q}, n, + \rangle$. Because the continuum in Fig. 5a is populated by different sets of discrete modes for the various system sizes considered, we choose to evaluate the degree of deconfinement through a single \mathbf{q} -specific averaged quantity

$$\rho_q(\mathbf{r}) = \sum_n \left| \langle \mathbf{q}, \mathbf{r}, + | \mathbf{q}, n, + \rangle \langle \mathbf{q}, n, + | S_q^+ |\text{SF}\rangle \right|^2 \quad (3)$$

where the aforementioned overlap is weighted by the intensity of the transverse spin excitation in the dynamic structure factor, thus only accounting for modes proportionally to their spectral weight. The spatial profile of $\rho_q(\mathbf{r})$ for the magnetic-zone-boundary wavevectors, shown in Fig. 1b,d, reveals much more extended fractional $S=1/2$ quasiparticles pairs at $(\pi, 0)$ than at $(\pi/2, \pi/2)$. This is confirmed by the system-size dependence of the radially integrated normalized distribution $P_q(r) = \sum_{|\mathbf{r}'| < r} \rho_q(\mathbf{r}')$, plotted in Fig. 5c,d. At $(\pi/2, \pi/2)$, $P_q(r)$ saturates at a distance, r , that is nearly independent of the system size, whereas at $(\pi, 0)$ it does

so at a distance that increases with the number of sites. Similarly, the ‘root-mean-square’ fractional quasiparticles pair separation $r_q = [\sum_r |\mathbf{r}|^2 \rho_q(\mathbf{r}) / \sum_r \rho_q(\mathbf{r})]^{1/2}$, presented in Fig. 5e, grows nearly linearly with the system size for $(\pi, 0)$, whereas it has a much weaker size dependence for $(\pi/2, \pi/2)$.

Taken together, our real-space results for the |SF⟩ state show that spin excitations at $(\pi/2, \pi/2)$ can indeed be considered as bound pairs of $S = 1/2$ quasiparticles with confined spatial extent. In contrast, at $(\pi, 0)$, the strong system-size dependence of the spin excitations spatial extent indicates the perhaps only marginal deconfinement of fractional quasiparticles in two spatial dimensions. Note that even in the absence of long-range Néel order, deconfinement happens only at the special point $(\pi, 0)$ and no continuum develops at (π, π) , as would be naively expected for an algebraic spin liquid. This indicates that the deconfined $(\pi, 0)$ excitations should be considered only as remnants of the underlying unprojected deconfined particle–hole excitations. This suggests that the QSLHAF ground state can still be understood as a conventional Néel state different from the AF* state described in refs 24,25, where magnons and spinons represent two different branches of excitations. We do not attempt to extract power laws from the numerical data, as the variational |SF⟩ state mimics the long-distance spin correlations only qualitatively.

Combining our polarized neutron scattering and theoretical results provides evidence that, even in the simplest of 2D spin models, deconfined fractional $S = 1/2$ quasiparticles can be identified at high energies, and account for the quantum anomaly observed in a broad range of experimental realizations of the square-lattice Heisenberg antiferromagnet. This insight raises important theoretical and experimental questions. First, how to obtain explicit quasiparticle deconfinement out of the magnetically ordered ground state of the QSLHAF? How will the excitations uncovered here evolve on weakening magnetic exchange in one direction, hence approaching the 1D limit? Our present work focused on the nearest-neighbour Heisenberg model, an insulator obtained in the strong Coulomb repulsion limit of a one-band Hubbard model. It will be interesting to track the fractional quasiparticles in systems closer to an insulator–metal transition, and eventually on doping. Given that fractional spin excitations are identified at high energies, one may speculate whether weak 2D Mott insulators could, in certain areas of momentum space, host a phenomenon similar to the observed spin-charge separation in 1D (ref. 62).

Received 10 April 2014; accepted 29 October 2014;
published online 23 December 2014

References

- Laughlin, R. B. Nobel lecture: Fractional quantization. *Rev. Mod. Phys.* **71**, 863–874 (1999).
- Su, W. P., Schrieffer, J. R. & Heeger, A. J. Solitons in polyacetylene. *Phys. Rev. Lett.* **42**, 1698–1701 (1979).
- Hou, C.-Y., Chamon, C. & Mudry, C. Electron fractionalization in two-dimensional graphene like structures. *Phys. Rev. Lett.* **98**, 1698–1701 (1979).
- Simon, J. *et al.* Quantum simulation of antiferromagnetic spin chains in an optical lattice. *Nature* **472**, 307–312 (2011).
- Baskaran, G., Zou, Z. & Anderson, P. W. The resonating valence bond state and high- T_c superconductivity—a mean field theory. *Solid State Commun.* **63**, 973–976 (1987).
- Balents, L. Spin liquids in frustrated magnets. *Nature* **464**, 199–208 (2010).
- Bethe, H. Zur Theorie der Metalle. *Z. Phys. A* **71**, 205–226 (1931).
- Faddeev, L. & Takhtajan, L. What is the spin of a spin wave? *Phys. Lett. A* **85**, 375–377 (1981).
- Müller, G., Thomas, H., Beck, H. & Bonner, J. C. Quantum spin dynamics of the antiferromagnetic linear chain in zero and nonzero magnetic field. *Phys. Rev. B* **24**, 1429–1467 (1981).
- Tennant, D. A., Cowley, R. A., Nagler, S. E. & Tsvetlik, A. M. Measurement of the spin-excitation continuum in one-dimensional KCuF_3 using neutron scattering. *Phys. Rev. B* **52**, 13368–13380 (1995).
- Mourigal, M. *et al.* Fractional spinon excitations in the quantum Heisenberg antiferromagnetic chain. *Nature Phys.* **9**, 435–441 (2013).
- Coldea, R., Tennant, D. A., Tsvetlik, A. M. & Tylczynski, Z. Experimental realization of a 2D fractional quantum spin liquid. *Phys. Rev. Lett.* **86**, 1335–1338 (2001).
- Han, T.-H. *et al.* Fractionalized excitations in the spin-liquid state of a kagome-lattice antiferromagnet. *Nature* **492**, 406–410 (2012).
- Jeong, M. *et al.* Field-induced freezing of a quantum spin liquid on the kagome lattice. *Phys. Rev. Lett.* **107**, 237201 (2011).
- Kozlenko, D. P. *et al.* From quantum disorder to magnetic order in an $S = 1/2$ kagome lattice: A structural and magnetic study of herbertsmithite at high pressure. *Phys. Rev. Lett.* **108**, 187207 (2012).
- Manousakis, E. The spin-1/2 Heisenberg antiferromagnet on a square lattice and its application to the cuprous oxides. *Rev. Mod. Phys.* **63**, 1–62 (1991).
- Canali, C. M. & Wallin, M. Spin–spin correlation functions for the square-lattice Heisenberg antiferromagnet at zero temperature. *Phys. Rev. B* **48**, 3264–3280 (1993).
- Reger, J. D. & Young, A. P. Monte Carlo simulations of the spin-1/2 Heisenberg antiferromagnet on a square lattice. *Phys. Rev. B* **37**, 5978–5981 (1988).
- Hamer, C. J., Weihong, Z. & Arndt, P. Third-order spin-wave theory for the Heisenberg antiferromagnet. *Phys. Rev. B* **46**, 6276–6292 (1992).
- Anderson, P. W., Baskaran, G., Zou, Z. & Hsu, T. Resonating valence-bond theory of phase transitions and superconductivity in La_2CuO_4 -based compounds. *Phys. Rev. Lett.* **58**, 2790–2793 (1987).
- Auerbach, A. & Arovas, D. P. Spin dynamics in the square-lattice antiferromagnet. *Phys. Rev. Lett.* **61**, 617–620 (1988).
- Hsu, T. C. Spin waves in the flux-phase description of the $S = 1/2$ Heisenberg antiferromagnet. *Phys. Rev. B* **41**, 11379–11387 (1990).
- Ho, C.-M., Muthukumar, V. N., Ogata, M. & Anderson, P. W. Nature of spin excitations in two-dimensional Mott insulators: Undoped cuprates and other materials. *Phys. Rev. Lett.* **86**, 1626–1629 (2001).
- Balents, L., Fisher, M. P. A. & Nayak, C. Dual order parameter for the nodal liquid. *Phys. Rev. B* **60**, 1654–1667 (1999).
- Ghaemi, P. & Senthil, T. Néel order, quantum spin liquids, and quantum criticality in two dimensions. *Phys. Rev. B* **73**, 054415 (2006).
- Greven, M. *et al.* Neutron scattering study of the two-dimensional spin- $S = 1/2$ square-lattice Heisenberg antiferromagnet $\text{Sr}_2\text{CuO}_2\text{Cl}_2$. *Z. Phys. B* **96**, 465–477 (1995).
- Plumb, K. W., Savici, A. T., Granroth, G. E., Chou, F. C. & Kim, Y.-J. High-energy continuum of magnetic excitations in the two-dimensional quantum antiferromagnet $\text{Sr}_2\text{CuO}_2\text{Cl}_2$. *Phys. Rev. B* **89**, 180410 (2014).
- Coldea, R. *et al.* Spin waves and electronic interactions in La_2CuO_4 . *Phys. Rev. Lett.* **86**, 5377–5380 (2001).
- Headings, N. S., Hayden, S. M., Coldea, R. & Perring, T. G. Anomalous high-energy spin excitations in the high- T_c superconductor-parent antiferromagnet La_2CuO_4 . *Phys. Rev. Lett.* **105**, 247001 (2010).
- Kim, Y. J. *et al.* Neutron scattering study of $\text{Sr}_2\text{Cu}_3\text{O}_4\text{Cl}_2$. *Phys. Rev. B* **64**, 024435 (2001).
- Tsyrulin, N. *et al.* Quantum effects in a weakly frustrated $S = 1/2$ two-dimensional Heisenberg antiferromagnet in an applied magnetic field. *Phys. Rev. Lett.* **102**, 197201 (2009).
- Tsyrulin, N. *et al.* Two-dimensional square-lattice $S = 1/2$ antiferromagnet $\text{Cu}(\text{Pz})_2(\text{ClO}_4)_2$. *Phys. Rev. B* **81**, 134409 (2010).
- Rønnow, H. M. *et al.* Spin dynamics of the 2D spin-1/2 quantum antiferromagnet copper deuteroformate tetradeuterate (CFTD). *Phys. Rev. Lett.* **87**, 037202 (2001).
- Christensen, N. B. *et al.* Quantum dynamics and entanglement of spins on a square lattice. *Proc. Natl Acad. Sci. USA* **104**, 15264–15269 (2007).
- Singh, R. R. P. & Gelfand, M. P. Spin-wave excitation spectra and spectral weights in square lattice antiferromagnets. *Phys. Rev. B* **52**, R15695–R15698 (1995).
- Zheng, W., Oitmaa, J. & Hamer, C. J. Series studies of the spin-1/2 Heisenberg antiferromagnet at $T = 0$: Magnon dispersion and structure factors. *Phys. Rev. B* **71**, 184440 (2005).
- Syljuåsen, O. F. & Rønnow, H. M. Quantum renormalization of high-energy excitations in the 2D Heisenberg model. *J. Phys. Condens. Matter* **12**, L405–L408 (2000).
- Sandvik, A. W. & Singh, R. R. P. High-energy magnon dispersion and multimagnon continuum in the two-dimensional Heisenberg antiferromagnet. *Phys. Rev. Lett.* **86**, 528–531 (2001).
- Lüscher, A. & Läuchli, A. M. Exact diagonalization study of the antiferromagnetic spin-1/2 Heisenberg model on the square lattice in a magnetic field. *Phys. Rev. B* **79**, 195102 (2009).
- Guarise, M. *et al.* Measurement of magnetic excitations in the two-dimensional antiferromagnetic $\text{Sr}_2\text{CuO}_2\text{Cl}_2$ insulator using resonant X-ray scattering: Evidence for extended interactions. *Phys. Rev. Lett.* **105**, 157006 (2010).

41. Dalla Piazza, B. *et al.* Unified one-band Hubbard model for magnetic and electronic spectra of the parent compounds of cuprate superconductors. *Phys. Rev. B* **85**, 100508 (2012).
42. Ishii, K. *et al.* High-energy spin and charge excitations in electron-doped copper oxide superconductors. *Nature Commun.* **5**, 3714 (2014).
43. Braicovich, L. *et al.* Magnetic excitations and phase separation in the underdoped $\text{La}_{2-x}\text{Sr}_x\text{CuO}_4$ superconductor measured by resonant inelastic X-ray scattering. *Phys. Rev. Lett.* **104**, 077002 (2010).
44. Zhitomirsky, M. E. & Chernyshev, A. L. Colloquium: Spontaneous magnon decays. *Rev. Mod. Phys.* **85**, 219–242 (2013).
45. Tang, Y. & Sandvik, A. W. Confinement and deconfinement of spinons in two dimensions. *Phys. Rev. Lett.* **110**, 217213 (2013).
46. Kohno, M., Starykh, O. A. & Balents, L. Spinons and triplons in spatially anisotropic frustrated antiferromagnets. *Nature Phys.* **3**, 790–795 (2007).
47. Enderle, M. *et al.* Two-spinon and four-spinon continuum in a frustrated ferromagnetic spin-1/2 chain. *Phys. Rev. Lett.* **104**, 237207 (2010).
48. Gros, C. Superconductivity in correlated wave functions. *Phys. Rev. B* **38**, 931–934 (1988).
49. Gros, C. Physics of projected wavefunctions. *Ann. Phys.* **189**, 53–88 (1989).
50. Li, T. & Yang, F. Variational study of the neutron resonance mode in the cuprate superconductors. *Phys. Rev. B* **81**, 214509 (2010).
51. Dmitriev, D. V., Krivnov, V. Y., Likhachev, V. N. & Ovchinnikov, A. A. Variation function with vortexes in the Heisenberg 2-dimensional antiferromagnetic model. *Phys. Solid State* **38**, 397 (1996) [Translated: *Fiz. Tverd. Tela* **38**, 397 (1996)].
52. Wen, X.-G. & Lee, P. A. Theory of underdoped cuprates. *Phys. Rev. Lett.* **76**, 503–506 (1996).
53. Nayak, C. Density-wave states of nonzero angular momentum. *Phys. Rev. B* **62**, 4880–4889 (2000).
54. Lee, T. K. & Feng, S. Doping dependence of antiferromagnetism in La_2CuO_4 : A numerical study based on a resonating-valence-bond state. *Phys. Rev. B* **38**, 11809–11812 (1988).
55. Trivedi, N. & Ceperley, D. M. Ground-state correlations of quantum antiferromagnets: A Green-function Monte Carlo study. *Phys. Rev. B* **41**, 4552–4569 (1990).
56. Calandra Buonaura, M. & Sorella, S. Numerical study of the two-dimensional Heisenberg model using a Green function Monte Carlo technique with a fixed number of walkers. *Phys. Rev. B* **57**, 11446–11456 (1998).
57. Liu, Z. & Manousakis, E. Variational calculations for the square-lattice quantum antiferromagnet. *Phys. Rev. B* **40**, 11437–11440 (1989).
58. Franjic, F. & Sorella, S. Spin-wave wave function for quantum spin models. *Prog. Theor. Phys.* **97**, 399–406 (1997).
59. Paramakanti, A., Randeria, M. & Trivedi, N. High- T_c superconductors: A variational theory of the superconducting state. *Phys. Rev. B* **70**, 054504 (2004).
60. Ivanov, D. A. Resonating-valence-bond structure of Gutzwiller-projected superconducting wave functions. *Phys. Rev. B* **74**, 024525 (2006).
61. Syromyatnikov, A. V. Spectrum of short-wavelength magnons in a two-dimensional quantum Heisenberg antiferromagnet on a square lattice: Third-order expansion in $1/S$. *J. Phys. Condens. Matter* **22**, 216003 (2010).
62. Kim, C. *et al.* Observation of spin-charge separation in one-dimensional SrCuO_2 . *Phys. Rev. Lett.* **77**, 4054–4057 (1996).

Acknowledgements

We gratefully acknowledge fruitful discussions with C. Broholm, L. P. Regnault, S. Sachdev and M. Zhitomirsky. Work in EPFL was supported by the Swiss National Science Foundation, the MPBH network, and European Research Council grant CONQUEST. The work of D.A.I. was supported by the Swiss National Foundation through the NCCR QSIT. Computational work was supported by the Swiss National Supercomputing Center (CSCS) under project ID s347. Work at Johns Hopkins University was supported by the US Department of Energy, Office of Basic Energy Sciences, Division of Material Sciences and Engineering under grant DE-FG02-08ER46544. N.B.C. was supported by the Danish Agency for Science, Technology and Innovation under DANSCATT.

Author contributions

B.D.P. and D.A.I. performed the theoretical work. B.D.P. wrote and ran the numerical calculations. M.M., N.B.C., M.E. and T.G.P. performed the experiments. G.J.N., P.T.-P. and N.B.C. grew the samples. M.M. analysed the data guided by M.E., N.B.C. and H.M.R. B.D.P., M.M., D.A.I. and H.M.R. wrote the paper with contributions from all co-authors. D.F.M., D.A.I. and H.M.R. supervised the project.

Additional information

Supplementary information is available in the [online version of the paper](#). Reprints and permissions information is available online at www.nature.com/reprints. Correspondence and requests for materials should be addressed to B.D.P. or M.M.

Competing financial interests

The authors declare no competing financial interests.